On the influence of bed permeability on flow in the leeside of coarse-grained bedforms

G. Blois [(1)], J. L. Best [(1)], G. H. Sambrook Smith [(2)], R. J. Hardy [(3)]

1 University of Illinois, Urbana-Champaign, Illinois, USA - blois@illiois.edu; jimbest@illinois.edu
2 University of Birmingham, Birmingham, UK - g.smith.4@bham.ac.uk
3 Durham University, Durham, UK - r.j.hardy@durham.ac.uk

Abstract
This paper details the dynamics of coherent flow structures generated in shallow flows *around* impermeable and permeable 2-dimensional bedforms overlaying a highly-permeable idealised bed. Particle imaging velocimetry (PIV) measurements were conducted in order to characterise flow both over and underneath idealised 2-dimensional dunes overlaying a packed bed of uniform size spheres. Experiments were conducted in free surface flow conditions (Froude number = 0.1; Reynolds number = 25,000) for one bedform height: flow depth ratio (0.31). The flow above the dune was measured using a standard PIV technique while a novel endoscopic PIV (EPIV) system allowed collection of flow data within the pore spaces beneath the dune. These results show that the permeability of the bed has a critical impact on flow around the bedform, inducing a significant interaction between the freeflow and subsurface flow. The interaction between the free-flow and hyporheic flow is significant; in the leeside, recirculation in the separation zone is replaced by a mechanism of asymmetric alternate vortex shedding. The paper will discuss the implications of these results for the morphodynamics of coarse-sediment bedforms.

1. BACKGROUND

In many natural shallow channel flows, the deposition of sediment creates a complex bedform geometry that provides both resistance to flow and can dominate the flow structure. This is witnessed by the presence of a multitude of bedforms in nearly all river channels, and by the presence of bedforms of different size, shape and internal structure, dependent on the grain size distribution of the bed sediment and the flow characteristics. Even though in most natural channels the bed can be regarded as permeable, many previous experimental, numerical and theoretical studies have treated such surfaces as essentially impermeable. However, the deposition of cohesionless sediments generates porous layers in which the permeability may be relatively high (especially in gravel-sized sediments) and, more importantly for shallow flows, where the subsurface flow may comprise a significant portion (up to 30-40%) of the total flow discharge. Recent large-eddy simulations (LES; Stoesser and Rodi, 2007) have shown that interactions between the freestream and subsurface flow of a highly permeable bed can dramatically alter the mechanisms of momentum exchange across the interface, and that this has direct implications for the stability of grains at the bed interface. These surface-subsurface flow interactions are expected to be even greater in the presence of bed topography that will generate pressure gradients at, and within, the bed surface. However, most models of bedform dynamics assume that the bed, and bedforms, are impermeable or characterized by laminar flows within the pore space (Cardenas and Wilson, 2007), and neglect the existence of any transitional layer in the upper sediment bed. The current lack of understanding of this transitional zone may be one of the reasons why the morphodynamics of coarse-grained bedforms are rather poorly understood.

Here, we investigate the role played by bed permeability on flow around an idealised bedform, in order to gain new insight on the formation and evolution of bedforms in cohesionless sediment. This paper details the dynamics of coherent flow structures generated around a model of a 2D impermeable bedform overlaying a permeable bed of cubically-packed uniform spheres (D = 0.04 m diameter). This simplified case of an isolated bedform concentrates on the structure and dynamics of the wake produced by such topography in the presence of bed permeability.

2. METHODOLOGY

Laboratory experiments were conducted in a recirculating hydraulic flume (Figure 1) that was 4.8 m long and had a cross-sectional width, W, = 0.35 m and height, H, = 0.60 m, in order to maximize the thickness (h_{bed}) of the permeable domain and the range of water depths (h_w) that could be investigated. Additional details on the flume characteristics, including flow conditioning and instrumentation can be found in Blois et al. (2011). For the present study, both h_{bed} and h_w were kept constant (h_{bed} = 0.24 m, h_w = 0.18 m), thus yielding a flow depth: bed thickness ratio, h_w/h_{bed}, of 0.75. The sediment bed, which covered the entire length and width of the flume test section, was built using a simplified geometry comprising six layers of uniform spheres (D = 0.04 m diameter) that were rigidly fixed in a cubic arrangement. A 2D bedform with a triangular cross-section (length, L_d = 0.41 m and height h_d= 0.056 m, with a leeside angle, α_{lee}, = 27°) was used. The grain roughness and bedform submergence were $h_w/(D/2) = 9$ and $h_w/h_d \approx 3.2$ respectively, this simulating a simplified dune in such coarse-grained sediment. The total flow discharge, Q_t, = Q_{bed} + Q_{stream} (see definitions below) was measured using a magnetic flow meter in the return pipe to the pump. An ultrasonic Doppler velocimetry profiler (UDVP) was used to measure the mean velocity of the freestream flow, U_0, for a number of flow conditions. The mean flow discharge over the bed, Q_{stream}, was estimated as $Q_{stream}=U_0 \cdot h_w \cdot W$. The flow uniformity over the permeable bed was characterised (without the bedform) by collecting UDVP data for different flow conditions and at different locations. Flow uniformity was achieved at a distance approximately 2 m downstream from the inlet section. Due to constraints in the experimental set-up, the measurement location was kept unchanged while the location of the bedform was varied to maximise the number of flow regions investigated. The bedform was placed in the flume at variable distances from the inlet section in the range 2.2 – 3.6 m, and in which the oncoming flow was uniform.

U_0 was also used to compute the freestream flow Reynolds number, $Re_s = U_0 \cdot h_w/\nu$ (where ν is the kinematic viscosity = $1.004 \cdot 10^{-6}$ m$^2 \cdot$s^{-1}) and Froude number $Fr_s = U_0 \cdot (g \cdot h_w)^{-0.5}$ (where g is acceleration due to gravity = 9.81 m$\cdot$s^{-2}). For the data reported herein, these dimensionless numbers are $2.1 \cdot 10^4$ and 0.18 respectively.

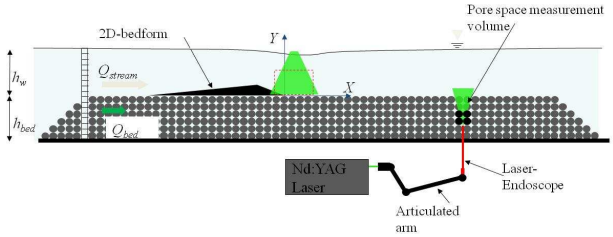

Figure 1. Schematic diagram of the experimental set-up.

The flume was instrumented with two different PIV systems: i) a standard PIV for above-bed measurements, and ii) an endoscopic PIV system (EPIV) for subsurface measurements (Fig. 1) as described in Blois et al. (2011). A photograph of the experimental set-up showing the solid dune placed on the permeable bed and both PIV systems is shown in Fig. 2. Above the bed, the flow was illuminated by a 50 mJ Nd:YAG laser (Litron Lasers) and was imaged by a 4 Mp camera (Redlake MotionPro Y5). Image capture was kept constant at 10Hz, thus obtaining time-resolved flow fields while allowing sufficient images (n = 2000, time series was tested for stationarity) to be collected to obtain robust statistics. The laser light was introduced from the top (see Fig. 1) as the water surface was relatively flat and the laser light could be provided in this configuration without any major refraction. For the subsurface flow, a two-borescope configuration was employed (Blois et al., 2011), with the seeding particles and image interrogation/ validation schemes being the same as those used for EPIV (see details in Blois et al. 2011).

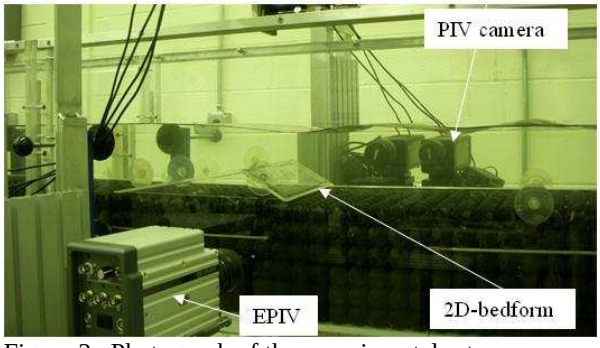

Figure 2. Photograph of the experimental set-up.

3. RESULTS

Figure 3 shows the time-averaged flow in the leeside of the impermeable bedform overlaying a highly-permeable bed. Our PIV data reveal that the wake generated in such a bed configuration is dramatically different when compared to classical cases of 2D impermeable bedforms on an impermeable bed (see review in Best, 2005). Specifically, our data show that: a) the flow separating at the crest does not reattach at the bed due to its interaction with flow in the near-bed region, which is characterized by continuous upwelling; b) this flow upwelling is so intense that it produces flow separation from the individual spheres, as suggested by the streamlines reported in Fig. 3; c) as a result of b), the flow separation zone, a major feature associated with flow transverse bedforms on beds that are impermeable, is absent and replaced by two large-scale counter-rotating vortices of comparable size; and d) the magnitude of vorticity is high both at the crest *and* at the toe of the bedform, thus highlighting the presence of two counteracting shear layers with opposite vorticity.

Figures 4 and 5 illustrate the mean flow *around* the bedform, meaning that flow both above *and* below the bedform was quantified. Pore space flow was collected using EPIV at 15 different X locations, at the same depth within the bed ($Y = -2D$). By examining Figs 4 (v component) and 5 (u component), we identified four different subsurface flow regions, herein termed A, B, C and D. This classification was based upon qualitative criteria that considered flow structure, velocity magnitude and the principal flow direction in the pore space. Region A is characterized by downward-moving flow that is generated by the high-pressure region upstream of the bedform. In region B, the flow can be mainly considered horizontal and flowing parallel to the bed surface. In region C, however, the pore flow has a strong upward-component, which is consistent with flow towards the low-pressure region above the bed associated with the bedform wake, which induces significant suction of the subsurface flow. Finally, region D has an upward-moving component but, contrary to regions A-C, the horizontal component is significantly negative. The relative extent of these regions highlights changes in the large-scale flow paths that are due to the specific bedform used. In all the pore space locations considered herein, the pore flow has high velocities and turbulence intensities ($Re_p > 300$, with $Re_p = U_p \cdot D/\nu$, where U_p is the mean pore space velocity magnitude). This onset of turbulence within the subsurface contrasts with recent numerical models that are based upon the assumption of a laminar subsurface flow (Cardenas & Wilson, 2007). In our present results, the mutual interaction between the turbulent wake and subsurface flow appears significant in the mechanisms governing these phenomena. Additional evidence to suggest that previous numerical methods may provide incorrect results can be found in the location of the low-pressure peak. Numerical models predict that the peak of low-pressure occurs very close to the crest (Cardenas & Wilson, 2007). The location of the peak in low pressure, qualitatively inferred from our velocity data by considering the direction and magnitude of the flow, is shown in Fig. 4. The data suggest that this low-pressure peak may be shifted downstream and that the distance between this peak and the bedform crest scales with the bed permeability. The existence of strong upstream-moving flow (region D) at a relatively long distance from the bedform supports this hypothesis. The effects observed at the bedform may also be influenced by grain roughness as well as bedform permeability, and thus additional experiments are needed in which these features of the bedform are isolated.

Figure 4 shows a very strong jet concentrated at the toe of the impermeable bedform and directed at 45 degrees up into the flow, while the flow upwelling progressively decreases in its magnitude downstream. These observations are supported by the patterns of subsurface flow, which show that the magnitude and distribution of upward-moving flow in the subsurface (region C) is proportional to the v component of the freestream flow at the same vertical location.

Figure 5 illustrates that the wake is characterized by a low-momentum region that is consistent with deceleration of flow in the subsurface.

The mean flow structure described above is the result of complex dynamic mechanisms taking place in the wake and involving the interaction between two shear layers of opposite vorticity. Figure 6 shows an example of the instantaneous flow fields in the wake of the bedform. Similar to

past descriptions of flow over backward-facing negative steps and bedforms, the shear layer originating at the crest generates clockwise-rotating vortices that tend to dominate the wake. However, in the case reported herein, the wake is dominated by a quasi-vertical jet that originates at the toe of the bedform (Fig. 6) and impinges against the clockwise vortices generated above near the bedform crest (see label A in Fig. 6). The jet dynamics are complex, involving pulsations and flapping dominating the motion in region A. In turn, the jet originating at the bed generates anticlockwise rotating vortices at the bedform toe (see B in Fig. 6) that subsequently interact with the vortices shed from the crest. The flow dynamics observed herein can thus be described as *asymmetrical vortex shedding*, since the vortex at the bedform toe (B) remains confined to the lee side, and only vortices generated at the crest (A) are shed downstream. Further downstream, the wake is dominated by larger-scale clockwise rotating vortices (C) that originate through the interaction between vortex A and the jet.

4. CONCLUSIONS

The present results show that the permeability of the bed has a marked impact on flow around the bedform, inducing a significant interaction between the freeflow and subsurface flow. As expected, the high pressure region generated on the stoss side of the bedform acts to force flow through the bed, whilst the low pressure region in the leeside induces an upwelling of fluid from the bed *into* the free flow. This upwelling flow in the leeside dramatically changes the dynamics of flow in the wake of the bedform. Bed permeability is thus shown to control the dynamics of coherent flow structures generated in the leeside and near-wake region of these porous, coarse-grained, bedforms.

The main findings of this paper are:

1) Flow upwelling in the bedform leeside appears in the form of pulsating jets, which are particularly intense at the toe of the bedform leeside and gradually decrease in their effect downstream.

2) Flow in the separation zone is dominated by a mechanism of asymmetric, *alternate*, vortex shedding that appears to trigger pulsing jet motions from the bed.

3) Three discrete flow regions can be identified *within* the bed: i) upstream of the bedform (region A): downward-moving flow is deflected downstream with significant horizontal flow accelerations; ii) beneath the bedform (region B): flow is predominantly horizontal and characterized by the interaction of multiple interacting jets, which results in a complex flow pattern; and iii) downstream of the bedform (regions C and D): pore space flow, although displaying a strong upward component, is predominantly directed diagonally, before converging at $x/D \sim 7$ and moving vertically upwards.

Based on these observations, it is suggested that the movement of fluid from the permeable bed *into* the freeflow may have a significant impact upon the recirculation zone in the wake of the bedform that has hitherto not been quantified, and will have considerable implications for the geometry and characteristics of bedforms generated in such coarse-grained, permeable, sediments.

5. REFERENCES

Best, J. 2005 Kinematics, topology and significance of dune-related macroturbulence: some observations from the laboratory and field. In: *Fluvial Sedimentology VII* (Eds. Blum, M.D., Marriott, S.B. & LeClair, S.), 41-60, Spec. Publ. Int. Assoc. Sediment., 35, Blackwells .

Blois, G., Sambrook Smith, G. H., Best, J. L. , Hardy, R.J. and Lead, J.R. (2011) Quantifying the dynamics of flow within a permeable bed using time-resolved endoscopic particle imaging velocimetry (EPIV). *Exp. in Fluids*, (in press) doi:10.1007/s00348-011-1198-8.

Cardenas, M.B. and Wilson J.L. (2007) Dunes, turbulent eddies, and interfacial exchange with permeable sediments. *Water Res. Research*, vol. 43, W08412, doi:10.1029/2006WR005787.

Stoesser, T. and Rodi W. (2007) Large eddy simulation of open-channel flow over spheres. *High Perform. Comput. Sci. Eng.*, vol. 4:321–330. doi:10.1007/978-3-540-36183-1_23.

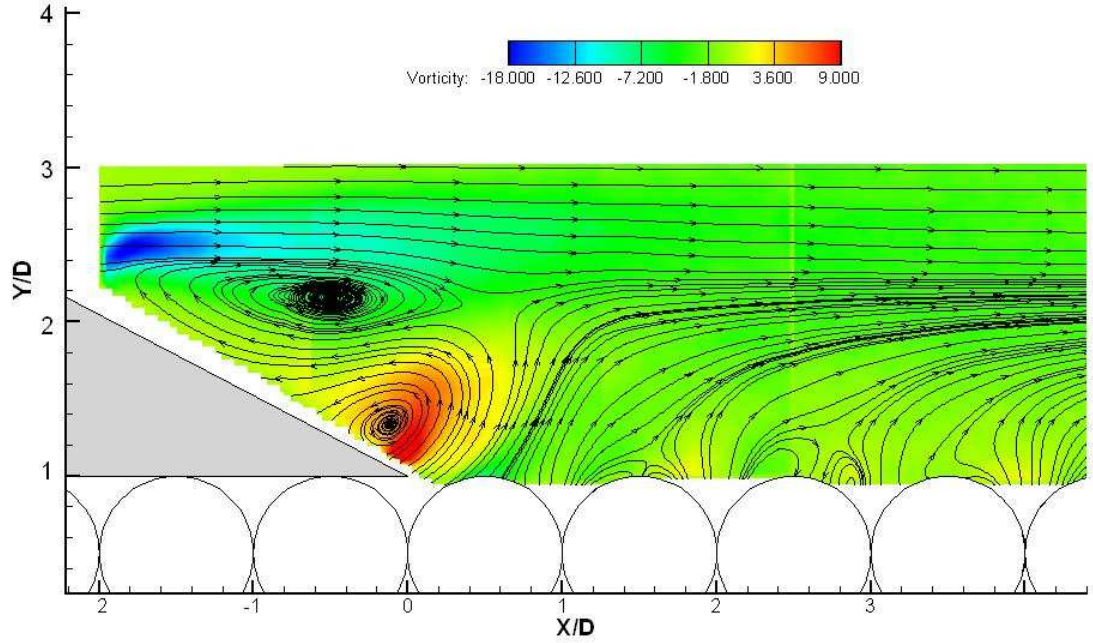

Figure 3. Mean flow in the leeside of an impermeable bedform showing the distribution of vorticity. Flow left to right. Streamlines are also shown to highlight the structure of the flow.

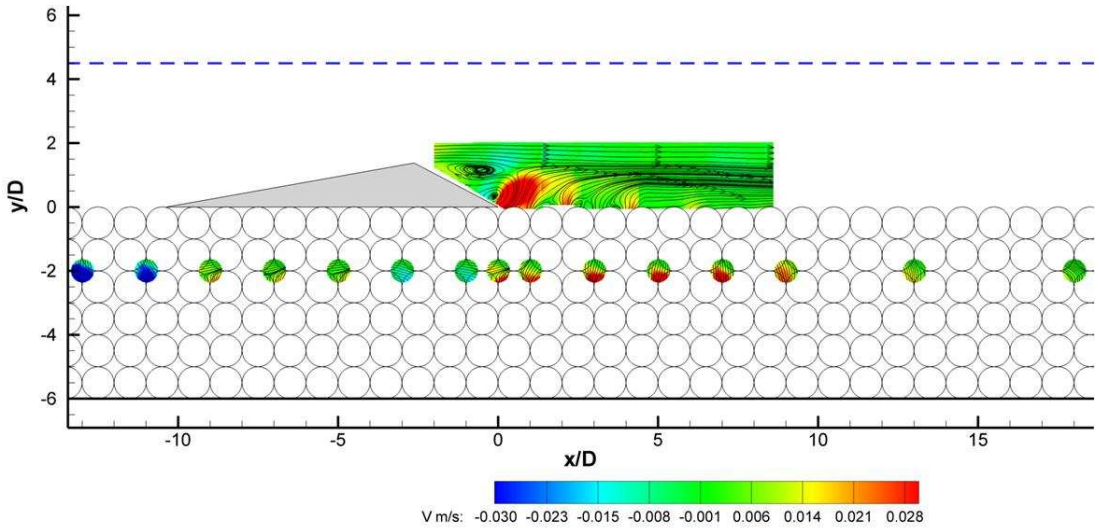

Figure 4. Distribution of *v* component around the bedform. The arrows on the figure represent the mean direction of the flow at the different pore space locations. The red dot represents the location of the low-pressure peak at the near bed.

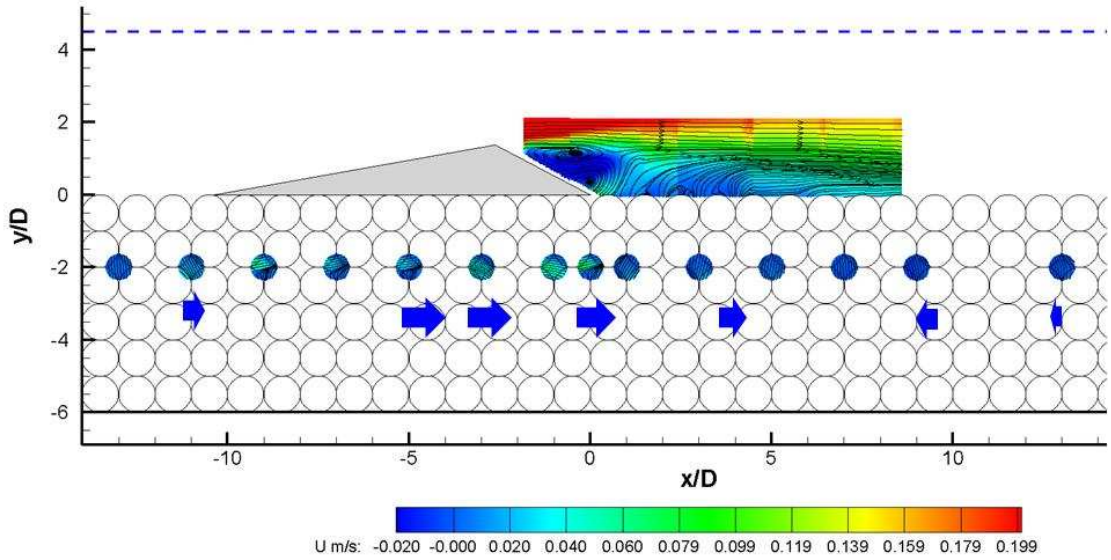

Figure 5. Distribution of *u* component around the bedform. The arrows on the figure represent the mean magnitude of *u* at the different pore space locations.

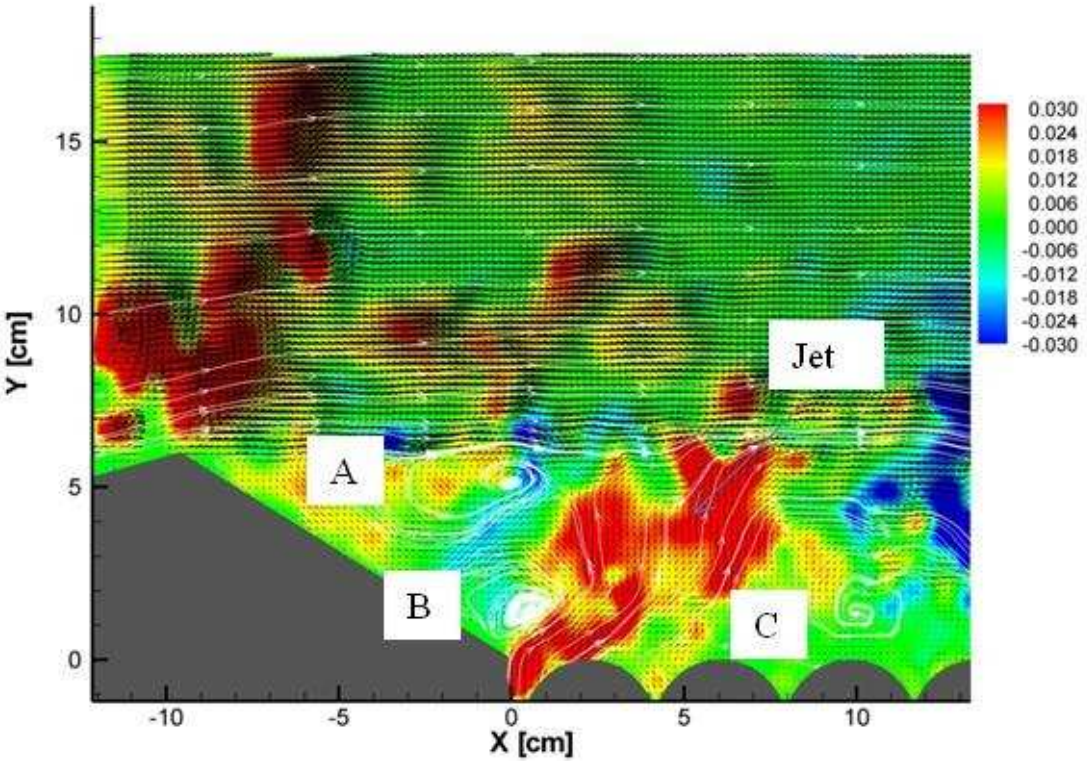

Figure 6: Example of instantaneous flow field in the bedform leeside, showing the *asymmetrical vortex shedding* mechanism. The colormap refers to the *v* component (ms^{-1}).